Reduced Symmetry Metallodielectric Nanoparticles: Chemical Synthesis and Plasmonic Properties†

Clarence Charnay,‡ Allen Lee,‡ Shi-Qing Man,‡ Cristin E. Moran,§ Corey Radloff,§ R. Kelley Bradley,|| and Naomi J. Halas*,‡,§

Department of Electrical and Computer Engineering and Department of Chemistry, Center for Nanoscale Science and Technology, Rice University, Houston, Texas, and Nanospectra L.L.C., Houston, Texas

Received: February 5, 2003; In Final Form: April 22, 2003

We report a general chemical strategy for producing reduced-symmetry metallodielectric nanoparticles, nanocups, and nanocaps that combines nanoscale masking techniques and nanoparticle-seeded electroless plating. Using this approach, silica nanoparticles with a gold cup-shaped shell and, alternatively, a gold cap, are obtained. The plasmon response of both nanostructures is a sensitive function of orientation of the nanostructure with respect to the direction and polarization of incident light. This orientation dependence is examined experimentally by studying the extinction spectra of oriented nanocups and nanocaps on transparent substrates, and is also evaluated theoretically using a three-dimensional finite difference time domain (FDTD) method.

Introduction

Metal nanostructures have been studied extensively in the field of nanoscience; their robust synthetic and functionalization chemistry, in combination with their interesting physical properties, make them ideal structures for fundamental research and applications. In particular, nanostructures made from the noble metals, (e.g. Au and Ag) with their associated strong plasmon resonance have generated great interest. The fact that the plasmon response is a sensitive function of nanostructure geometry, coupled with synthetic advances that allow for controlled and systematic variations in nanostructure geometries, is leading to a dramatic increase in interest in this topic. This renaissance is resulting in a new field called "plasmonics", associated with the design and fabrication of nanooptical components that focus and manipulate light at spatial dimensions far below the classical diffraction limit. New applications of plasmonics, such as metal nanostructure-based strategies for chemical sensing,[1,2] electromagnetic wave transport,[3,4] and the development of new optically responsive materials[5,6] have recently been reported. This is also stimulating an increased theoretical interest in the electronic and electromagnetic properties of mesoscopic metal structures.

From the variety of nanoscale geometries that have stimulated interest in plasmonics, a particular geometry of significant practical interest is a nanoshell: a metallodielectric nanoparticle where Au or Ag forms a uniform shell around a dielectric core. It has been shown that metallodielectric, core−shell nanoparticles possess a tunable plasmon resonance that can be controlled by changing the ratio of the core radius to the shell thickness.[7,8] The core/shell ratio of a nanoshell controls its far-field optical properties, so that its color can be tuned across the electromagnetic spectrum. It also controls the intensity of the optical field at the surface of the nanoparticle, enabling the control and optimization of Raman scattering enhancements at the nanoshell surface.[9,10] For Au−silica nanoshells, the nanoshell particle is constructed by first attaching small gold nanoparticles onto the surface of a silica nanoparticle. This is followed by the reduction of gold from solution onto the core utilizing the chemisorbed gold nanoparticles as nucleation sites. The resulting nanoshell possesses a frequency agile plasmon resonance that can be tuned from the visible to the infrared region of the electromagnetic spectrum.[11−13] Several other methods for the synthesis of core−shell nanostructures have been reported, which include growth of a metal shell onto core materials other than silica,[14,15] variations in reductant chemistry,[16] and the synthesis of hollow crystalline shells by templating on block copolymers.[17]

Reducing symmetry for the core−shell geometry does interesting things to the plasmon resonance of this nanostructure: the plasmon response becomes a sensitive function of the orientation of the nanostructure with respect to incident light. Both the plasmon frequency and the cross section of the response show a strong and dramatic orientation dependence. This unique property should make possible the orientation and manipulation of these nanostructures by applied electric and electromagnetic fields, which in turn should give rise to new plasmonic devices and applications.

Recent articles have reported the fabrication of reduced-symmetry nanoshells at an approximately 50% metal coverage by evaporation of metal onto dielectric nanoparticles deposited onto a substrate.[18] In this article we report a chemical strategy for synthesis of reduced-symmetry nanoparticles of two types: nanocups, with approximately 70−80% metal coverage, and nanocaps, the inverse structure, with approximately 20−30% metal coverage. Our approach combines nanoparticle deposition onto a substrate that provides a site for partial chemical passivation of the nanoparticle surface, followed by subsequent nanoshell nucleation and deposition chemistry to selectively coat a specific section of the nanostructure surface with metal. We also investigate the plasmon response of both nanocups and nanocaps as a function of nanoparticle orientation with respect to incident light and polarization angle. These results are

† Part of the special issue "Arnim Henglein Festschrift".

* Corresponding author: halas@rice.edu.
‡ Department of Electrical and Computer Engineering.
§ Department of Chemistry.
|| Nanospectra L.L.C.

10.1021/jp034309r CCC: $25.00
Published on Web 06/17/2003

compared quantitatively to theoretical calculations of the plasmon response using a three-dimensional finite difference time domain (FDTD) method developed for plasmonic nanostructures.[19] The synthetic approach demonstrated here results in nanostructures whose plasmon responses agree quite favorably with the theoretically predicted response of this nanostructure.

Experimental Procedure

Materials. Tetrakishydroxymethylphosphonium chloride (THPC; Aldrich), tetrachloroauric acid ($HAuCl_4$; Aldrich), potassium carbonate (K_2CO_3; Fluka), and formaldehyde (Aldrich) were used as received. Tetraethyl orthosilicate (TEOS; Aldrich) and 3-aminopropyltrimethoxysilane (APTS; Aldrich) were freshly distilled before use. Ammonium hydroxide (NH_4OH, Fluka; 29% NH_3), 200 proof grade ethanol (Pharmco), and Milli-Q water (Millipore) were all used in the synthesis of the silica particles. Glass microscope slides were used as substrates. Prior to use the slides were washed by boiling first in methanol, then in a peroxide solution with a few drops of NH_4OH. After boiling the slides were rinsed, and stored in Milli-Q water. Silicone elastomer (PDMS, Sylgard 184) was purchased from Dow Corning Corporation. The PDMS is mixed with the curing agent (10:1 v/v) and outgassed under low pressure (100 milliTorr) at ambient temperature for a half-hour before use.

Monodispersed silica particles were used as the core substrate in the preparation of gold nanocups and nanocaps. These particles were synthesized according to the Stöber method.[20,21] Following synthesis, the surface of the particles was functionalized with APTS using a previously described method.[22] Particle size distributions were measured from multiple TEM images using a JEOL JEM-2010 transmission electron microscope (TEM). Dynamic light scattering (DLS) was also used to determine particle size distribution. Silica particle solutions were diluted before use by adding 500 μL of the particle suspension to 20 mL of ethanol. Aqueous solutions of small gold nanoparticles (2−3 nm in diameter) were prepared by the reduction of chloroauric acid with THPC as detailed in the literature.[23]

Reduced-Symmetry Nanoparticle Preparation. Nanoparticles possessing a reduced symmetry geometry were prepared by adapting the procedure used for the preparation of silica core/gold nanoshells, which is described elsewhere.[11] The synthesis of these geometrically and chemically asymmetric particles was accomplished by masking one part of the particle surface to avoid the formation of a complete spherical gold shell. The process for the preparation of silica particles with asymmetric gold shells is illustrated in Figure 1. The process can be divided into three steps. The first step consists of masking a portion of the core particle surface. The amine-functionalized silica particles were deposited onto a substrate that masks the particle surface in contact with the substrate. This geometry limits the overall surface area of the particle that can be masked. To increase the masked surface area, the deposited particles can be embedded in a polymer matrix. The second step consists of the attachment of gold nanoparticles to the exposed silica particle surface. The final step is the growth of the desired gold shell by chemical reduction of gold hydroxide using formaldehyde as the reductant. The adsorbed gold nanoparticles act as nucleation sites for the gold salt reduction onto the silica core particle. The gold shell growth proceeds by mixing 50 μL of a formaldehyde solution (37 wt %) to 25 mL of a stock gold solution (3.5 mM $HAuCl_4$, 1.75 mM K_2CO_3).

Nanocup Preparation. To begin preparing metal nanocups, APTS-functionalized silica particles were first deposited onto a negatively charged glass slide from an aqueous solution at a pH of 4. Maintaining a solution pH of 4 keeps the particles isolated on the substrate during deposition. In this step the glass slide was kept in the diluted suspension for about 5 min, then removed and gently washed with water. The exposed surface of the particles was then coated with gold nanoparticles by immersing the slide in the gold colloid solution for about 4 h. The small gold colloid has a high affinity for the silica particles by attaching to the amine functional groups. The glass slide was then removed from the gold colloid solution and washed with water. Growth of the gold nanocup on the exposed part of the gold-decorated silica surface was accomplished by immersing the glass slide (with particles) into the stock gold solution followed by the addition of the reducing agent. It was necessary to repeat the reduction step until the glass slide became blue-green in color, indicating the formation of the gold nanocups. Between each gold reduction reaction the glass slide was washed with water.

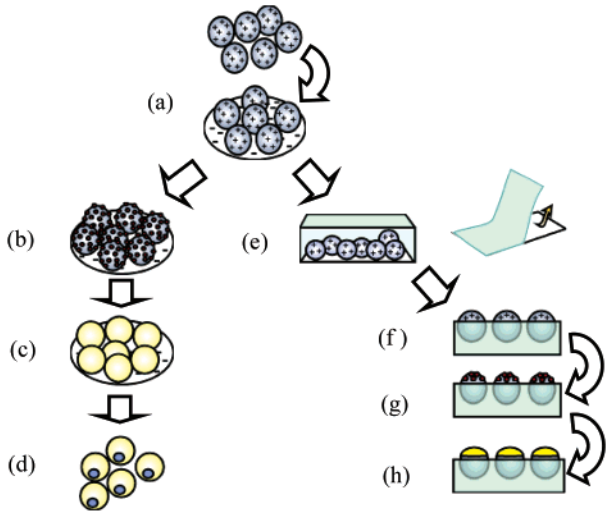

Figure 1. Schematic representation of the fabrication of reduced-symmetry nanoparticles. (a) APTS functionalized silica particles are deposited onto an oppositely charged substrate through electrostatic interaction. The region of the particles in contact with the substrate is thus masked for subsequent steps. (b) Particles are seeded for nanocup growth by immersing the immobilized particles into a solution of small gold nanoparticles. (c) The immobilized particles are then transferred to an electroless plating solution where the asymmetric shell is grown. (d) The immobilized particles can be released from the substrate using sonication. (e) Particles are prepared for nanocap growth by pouring PDMS over the immobilized particles. (f) Once cured, the PDMS can be peeled off the substrate, resulting in a PDMS film with partially embedded silica nanoparticles. (g) The embedded particles are then immersed into a solution of small gold nanoparticles. (h) The embedded particles are then immersed in an electroless plating solution where the asymmetric shell is grown.

The nanocup particles obtained in this manner could be removed from the substrate using probe sonication and dispersed in a suitable solvent such as water, ethanol, or DMF. After removal from the substrate, the nanocup particles were characterized using scanning electron microscopy (SEM). Figure 2 shows that each particle has a well-defined and uniform dark area where no gold has been reduced. This area corresponds to the region of the particles that had been masked by the substrate. The plasmon response of nanocups was studied without removing the particles from the substrate in order to preserve the nanoparticle orientation inherent in the fabrication process.

Nanocap Preparation. The preparation of nanocap particles follows the same initial particle deposition used in preparing nanocups. After washing and drying the glass slide, PDMS

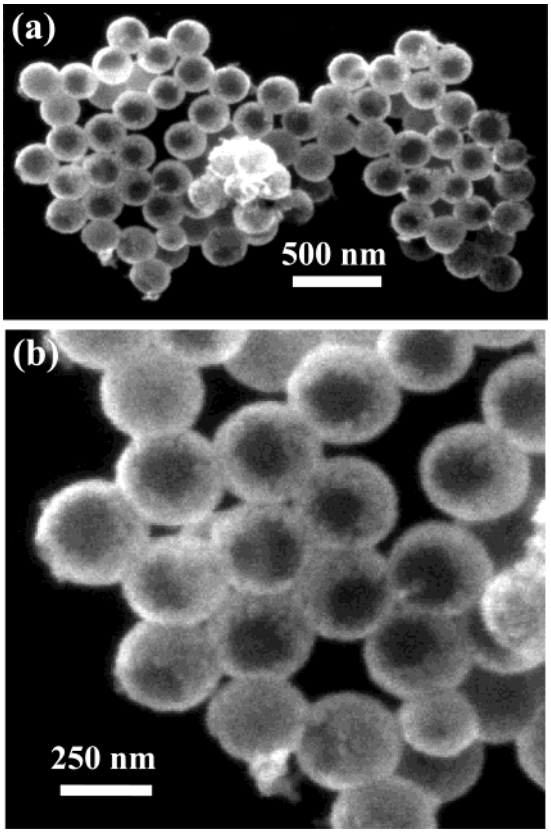

Figure 2. SEM images of gold nanocup particles. (a) Low magnification image showing randomly oriented nanocup particles. (b) High magnification image showing the nanocup geometry in closer detail.

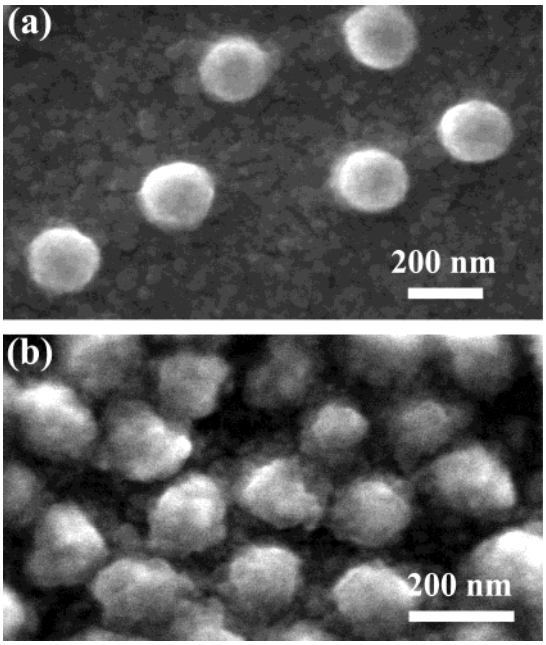

Figure 3. SEM images of the embedded silica particles (a) before and (b) after the growth of the gold nanocap.

elastomer was poured over the particles and left to stand for about 6 h at 323 K in order to cure the elastomer. The PDMS matrix had a typical thickness of about 1 mm. Upon removing this film from the substrate, it was observed that the silica particles were pulled off of the glass slide. As shown in Figure 3a, the silica particles were partially embedded in the PDMS and only a small part of their surface was exposed. In this way most of the particle surface is masked and cannot react under

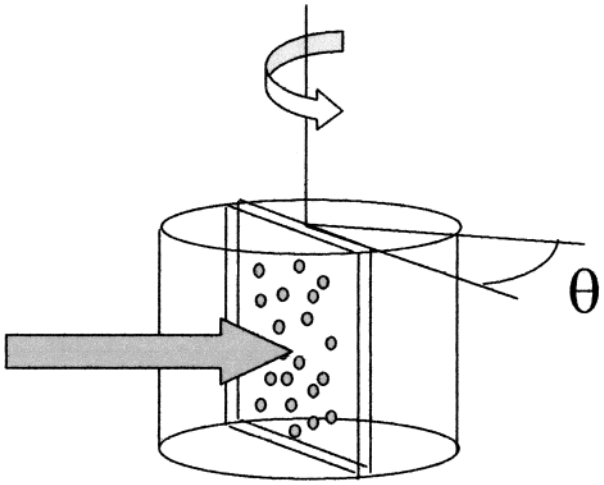

Figure 4. Schematic diagram of the sample collection geometry. The polarized light is incident on the sample at the axis of rotation, s-polarized light is along the rotation axis, p-polarized light is orthogonal to the rotation axis.

further processing. To attach the gold nanoparticles to the exposed surface of the silica particles, the PDMS film with the embedded silica particles was dipped for 48 h in the solution of gold colloid. Once the gold nanoparticles were attached, gold nanocap particles were obtained using the same reduction process as described for nanocups.

Figure 3b also shows an SEM image of gold-capped silica nanoparticles at the surface of the PDMS film. The surface of gold nanocaps appears rough in comparison to the embedded silica particles, Figure 3a. This roughness is characteristic of a metallic film that is chemically deposited. The gold nanocap arises from the growth of the previously adsorbed gold nanoparticles, which are used as nucleation sites during the reduction process. The size of these gold particles increases until they coalesce and form a continuous metallic structure. We observed a size distribution of nanocaps from 20 to 90 nm in diameter. The observed size distribution results from different parameters associated with the substrate preparation that will be discussed below. To measure the orientational dependent plasmon response of nanocaps, the particles were not removed from the elastomer film so as to preserve their structure and orientation on the substrate.

Optical Measurements

The optical spectra of nanocups and nanocaps were measured as a function of nanoparticle orientation with respect to incident p- and s-polarized light. The experimental geometry is shown in Figure 4. For this geometry, p-polarized light is defined with the electric field vector orthogonal to the axis of rotation of the measurement cell, and for s-polarized light the electric field vector is parallel to the axis of rotation of the measurement cell. The output of a halogen lamp was focused into a 0.25 m monochromator and polarized using a cube polarizer. The transmission spectra of the nanoparticle films were measured using a silicon photodiode detector and standard lock-in techniques. The samples were mounted inside a cylindrical glass cell containing uncured liquid PDMS elastomer to achieve index matching between the sample substrate and the walls of the cylindrical cell. A cured PDMS film was used as a reference. The extinction spectra of nanocups and nanocaps measured using p-polarized light were normalized for comparison. Normalization was made with respect to the peak intensity at 680

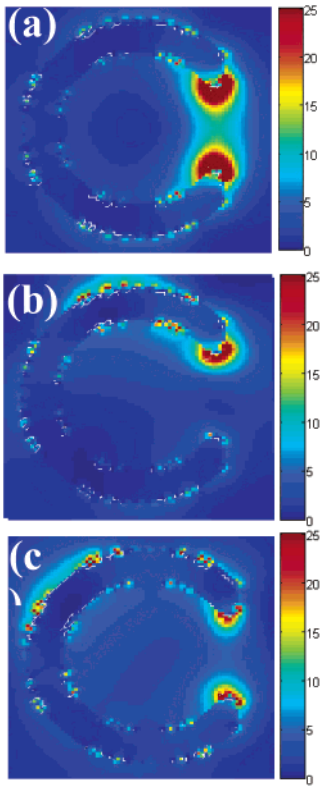

Figure 5. Theoretical calculations of the near field optical intensity ($|E|^2$) of nanocups. Nanocup plasmon resonance with incident illumination at (a) $\theta = 0°$ and $\lambda = 600$ nm, (b) $\theta = 40°$ and $\lambda = 600$ nm. (c) Nanocup short-axis plasmon resonance with incident illumination at $\theta = 80°$ and $\lambda = 600$ nm. The irregularities in the field strength near the surfaces of both structures are staircasing artifacts resulting from the FDTD spatial discretization.

nm of a nanoshell-embedded PDMS film measured using p-polarized light.

Discussion: Plasmon Response of Nanocups and Nanocaps

Nanocups. The near field intensities for gold nanocups are shown in Figure 5, as calculated using a three-dimensional finite difference time domain (FDTD) numerical method developed for the study of plasmonic nanostructures.[19−24] In this figure the near field distribution of a nanocup under resonant illumination for a range of orientations (0, 40, and 80 degrees) under p-polarized optical illumination with a silica core are shown. The cross-sectional plane corresponds to both the plane of polarization and the plane of incidence: for Figure 5a the light is incident from the left, and for Figure 5b,c the angle of incidence increases in the clockwise direction. The basic characteristics of a nanocup plasmon are readily apparent from this calculation. The highest field intensities are located at the metal cup edges, and by varying the angle with respect to incident light, the relative strength of the field along the metal cup edge is varied. This is seen most dramatically in Figure 5b where, for 40 degree excitation, the field intensity at the nearest edge of the nanocup is much greater than that at the far edge with respect to the direction of incidence. The plasmon response in both the near and far field is very similar whether the nanocup edge is facing the incident light or is opposite to the incident light, or rotated 180 degrees from the source (not shown). However, when the nanocup orientation is rotated from normal incidence (Figure 5a) to side incidence (Figure 5c), the plasmon response is noticeably blue-shifted.

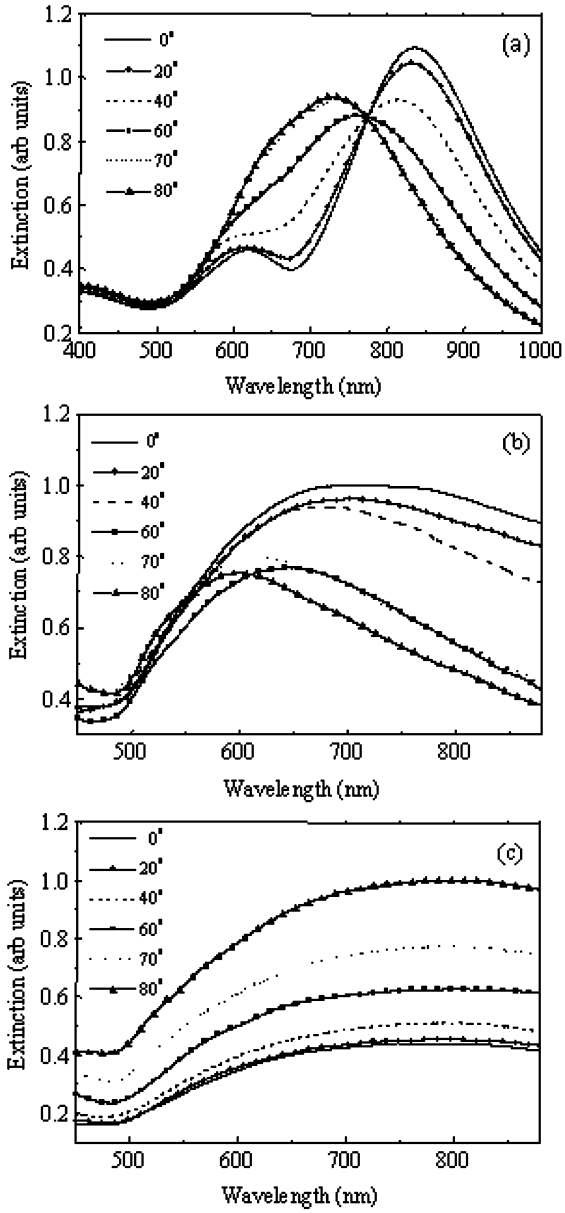

Figure 6. Angle dependent nanocup extinction spectra. (a) Theoretically calculated at various incident angles, θ, for the gold nanocup in Figure 5. The large peak at ~850 nm corresponds to the long-axis dipolar plasmon resonance; the peak at ~725 nm corresponds to the short-axis plasmon resonance. The small peak at ~610 nm for small angles is a quadropole resonance. Angle dependent nanocup extinction spectra measured with (b) p-polarized light and (c) s-polarized light.

The far field extinction spectra for gold nanocups as this orientation angle is changed are shown in Figure 6. Figure 6a shows the theoretically calculated extinction spectra for gold nanocups with a core radius $r = 50$ nm, a gold thickness $t = 20$ nm, and hole diameter $h = 50$ nm. The large peak centered at 830 nm corresponds to the long-axis dipolar plasmon resonance, and the peak centered at 725 nm corresponds to the short-axis plasmon resonance. The small peak at 610 nm for small angles is a quadrupole resonance. Figure 6b shows the experimental extinction spectra obtained using p-polarized light as the irradiation angle θ varies. Agreement with the theoretically predicted spectra in Figure 6a is not quantitative, but qualitatively a very similar angle-dependent frequency shift (~100 nm) in the plasmon response is clearly seen as the nanocup orientation is rotated from normal to side incidence. At normal incidence, $\theta = 0°$, the extinction spectrum exhibits

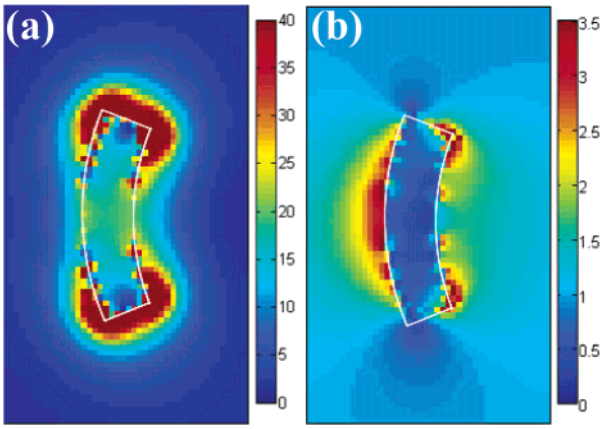

Figure 7. Theoretical calculations of the near field optical intensity ($|E|^2$) of nanocaps. (a) Nanocap longitudinal plasmon resonance with incident illumination at $\theta = 0°$ and $\lambda = 686$ nm. (b) Nanocap transverse plasmon resonance with $\theta = 90°$ and $\lambda = 515$ nm. The irregularities in the field strength near the surfaces of both structures are staircasing artifacts resulting from the FDTD spatial discretization.

a broad peak centered at approximately 700 nm. As the incident angle is increased, the intensity of this extinction peak decreases, and the peak position is blue shifted. At $\theta = 80°$, the peak has shifted to nominally 600 nm.

The discrepancies between the theoretical and experimental plasmon response are most likely attributable to the inherent roughness of the gold nanocup surface described in this work. The theoretical model that was used assumes a perfectly smooth shell, whereas a rough or porous shell would be expected to broaden the plasmon resonance, provide a smaller wavelength shift, and smooth out any multipolar features that may be present, specifically the appearance of the quadrupolar resonance. Figure 6c shows the experimental extinction spectra for nanocups using s-polarized light. For this polarization orientation there should be no angle dependence in the optical response of the nanostructures, since the **E** field of the incident wave is parallel to the axis of rotation and therefore does not change in orientation as the nanocup angle is changed. As θ is increased, no spectral shift is observed; however, the extinction intensity increases with increasing sample angle because a greater number of nanostructures are being illuminated within the optical beam with increasing angle.

Nanocaps. The near field intensities for gold nanocaps are shown in Figure 7, as calculated using a three-dimensional finite difference time domain (FDTD) numerical method. A cross-sectional slice of a nanocap is shown, and both the **E** and **k** vectors are in the plane of the figure. For Figure 7a, light is incident from the left, and for Figure 7b light is incident from below. Under these two excitation directions, two plasmon modes are selectively excited: a longer wavelength longitudinal plasmon as seen in Figure 7a and a shorter wavelength transverse plasmon mode shown in Figure 7b. The presence of polarization dependent longitudinal and transverse plasmon frequencies is also seen in nanorods and other elliptical nanostructures. In Figure 8, the theoretical and experimental extinction spectra for gold nanocaps are shown, and these two primary plasmon excitations are apparent. For normal incidence, only the longer wavelength longitudinal mode is excited; as the particle is rotated beyond 45 degrees the smaller wavelength, and smaller amplitude, transverse plasmon begins to appear. In both theory and experiment, the extinction spectra decrease as the orientation of the nanocap is rotated from normal incidence to sideways incidence. The extinction cross-section for sideways incident excitation is dramatically smaller than for normal incidence.

Figure 8a shows the theoretical extinction spectra of a gold nanocap with a cap size $d = 55$ nm, a core radius $r = 50$ nm, and a cap thickness $t = 12.5$ nm at various incident angles under p-polarized incident light. The theoretical spectra exhibit both a longitudinal plasmon resonance peak at 688 nm and a transverse plasmon resonance peak at 512 nm, which appears at larger angles. Moreover, the extinction intensity ratio of the transverse plasmon resonance relative to the longitudinal plasmon resonance increases with increasing incident angle. Figure 8b shows the experimental extinction spectra for oriented gold nanocaps. At normal incidence, $\theta = 0°$, the extinction spectrum exhibits a broad peak with a maximum at 708 nm, due to excitation of the longitudinal plasmon. As the incident angle increases, the intensity of this peak is consistently reduced until there is almost no extinction at $\theta = 80°$. At angles greater than $\theta = 60°$, a peak in the extinction spectrum at 540 nm, the shorter wavelength transverse plasmon, begins to appear. As the incident angle is increased, the ratio of the extinction intensity of the transverse plasmon resonance compared to the longitudinal plasmon resonance increases. As the angle is varied from 60 to 80 degrees, this ratio changes from 0.65 to 1.11. Except for the extinction bandwidth, which is much wider for the experimental measurements than for theory, there is a good qualitative agreement between the calculated and experimental extinction spectra: all major features are readily observable. As with nanocups, the theory assumes a perfectly smooth gold cap while the synthesis results in structures with a nanoscale roughness (Figure 3b). For nanocaps, the plasmon line width is also broadened inhomogeneously due to the size distribution of the fabricated nanocaps. The effect of this size distribution will be discussed below.

In Figure 8c,d, we report two important control experiments that illustrate the difference in optical response between nanocaps and nanoshells. Figure 8c shows the changing extinction spectra of a sparse, PDMS-embedded nanoshell film under p-polarized light as the incident angle θ is varied. The nanoshells were synthesized by a standard method[11] and subsequently deposited onto a glass slide so that their plasmon response could be compared directly to nanocups and nanocaps. For the case of the spherically symmetric nanoshells, one would not anticipate any angular dependence in the plasmon extinction spectrum, and indeed none is observed. The extinction increases with increasing angle, similar to the nanocup plasmon response, since at greater angles more nanoshells enter the beam spot of the experiment. For both nanoshells and nanocups, the inverse cosine angle dependence of the extinction amplitude that one would expect from geometrical considerations is observed. As the incident angle increases, the number of nanoshells or nanocaps being irradiated increases. This observation makes the nanocap angular response, which decreases with increasing angle of orientation, particularly striking in contrast. Figure 8d shows the extinction spectra of nanocaps under s-polarized light as the incident angle θ varies. The spectral features of the nanocap plasmon response under s-polarized light exhibit no angular dependence other than a changing intensity. However, in comparison with the p-polarized excitation of Figure 8a,b, the extinction intensity in Figure 8d increases with increasing incident angle, again with the same inverse cosine angle dependence anticipated from geometrical optics arguments.

For nanocaps, the spectral widths of the experimental extinction spectra are substantially broader than the peaks in

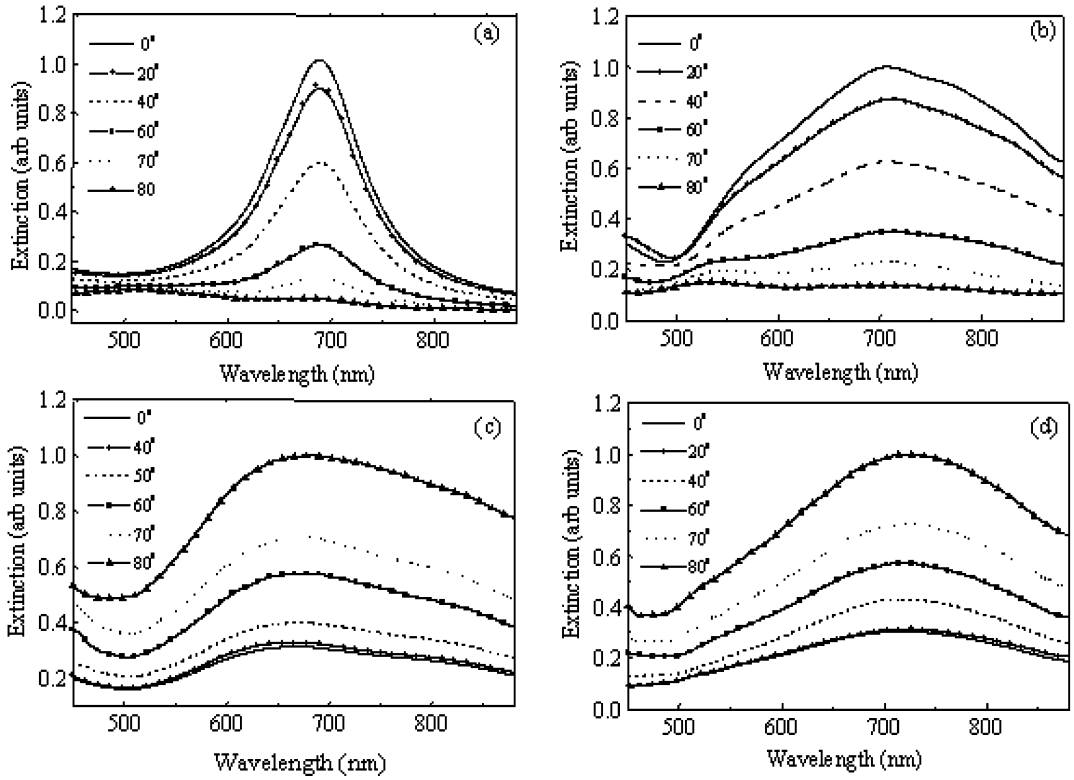

Figure 8. Angle dependent nanocap extinction spectra: (a) theoretically calculated and (b) measured for gold nanocaps as a function of orientation with respect to the incident light; both plots are for p-polarization. Note the small peak at ~500 nm that appears for large angles. Angle dependent extinction spectra (c) of nanocaps measured with s-polarized light and (d) of PDMS-embedded nanoshells measured with p-polarized light.

the corresponding theoretical spectra. This discrepancy can be accounted for if the experimentally fabricated nanocaps are assumed to exhibit a significant size distribution (Figure 9). Variations in the amount that the silica cores protrude from the PDMS masking layer result in a broad distribution of nanocap diameters, even when the silica nanoparticle cores are highly monodisperse. In this experiment the size distribution of the core silica nanoparticles was kept less than 5%.

Moreover, AFM measurements support the conclusion that the thickness of the gold cap is well defined and is nearly homogeneous over the entire nanocap sample. This homogeneous deposition of the nanoshell layer has also been inferred from plasmon line width studies of silica−gold nanoshells.[25] The heterogeneity of the nanocap diameters that results in the observed broadening of the nanocap plasmon line width relative to the theoretical predictions is mainly a consequence of the cap radius distribution rather than a cap thickness distribution. Several parameters account for this nanocap size distribution. First, the nanocap size distribution is linked to a variation in the amount of the silica core protruding from the PDMS matrix. The variation in the height of the nonmasked surface of the embedded silica nanoparticles depends on the flow of the noncured elastomer around the immobilized particles. Properties such as the viscosity of the liquid PDMS and its contact angle with the surface of the silica particle are important. The variation of the gold colloid coverage on the exposed part of the silica particle surface is another important parameter in understanding the cap size distribution. A poor coverage of gold colloid will hinder the growth and the coalescence of the metal cap. A decrease in the diffusion mobility of gold nanoparticles near the surface of the PDMS film may reduce the attachment of the gold colloid on the available surface of the partially embedded silica nanoparticles. Since the aqueous solution does not wet the PDMS, the approach of the gold colloid toward the PDMS surface where the silica nanoparticles are embedded may be arrested, as may the gold deposition from solution onto the nanocap structures.

To examine the effect of the size distribution of the gold nanocaps on the plasmon resonance, additional calculations of the plasmon response of nanocaps were performed for gold nanocaps of various sizes. In Figure 9a, theoretical extinction spectra are plotted for nanocaps with a core radius $r = 50$ nm, a gold cap thickness $t = 12.5$ nm, and various diameters d illuminated under normal incidence ($\theta = 0°$). As the diameter of the nanocap is increased, the long-axis dipole peak red shifts. Furthermore, the dependence of the plasmon resonance frequency on the cap diameter is approximately linear. The increase of the gold cap diameter while the gold thickness is kept constant represents an increase of the aspect ratio of the gold cap. This is associated with the red shift of the longitudinal mode of the plasmon. Similar results have been reported in investigations of other asymmetric gold nanoparticles such as nanorods.[26−29] Therefore, it can be expected that the experimental spectra in Figure 8b are a superposition of the longitudinal mode of the plasmon resonance for the different gold cap sizes that are present in the sample. Figure 9b illustrates the results of fitting the experimental spectrum from Figure 5a, $\theta = 0°$, with three theoretical spectra generated by assuming the nanocaps have a core radius $r = 50$ nm, a gold cap thickness $t = 12.5$ nm, and possess a distribution of diameters with $d = 25$, 55, and 85 nm. A variation of less than 15 nm in the height of the silica core protruding from the PDMS matrix before gold cap growth can account for the distribution in the diameter of the nanocaps. The effect due to a distribution in cap thickness was examined but found to have only a minor effect on the peak plasmon position relative to a distribution in cap diameter. This agrees well with the known variation in the elastomer surface as determined by microscopy. The mean maximum height of this

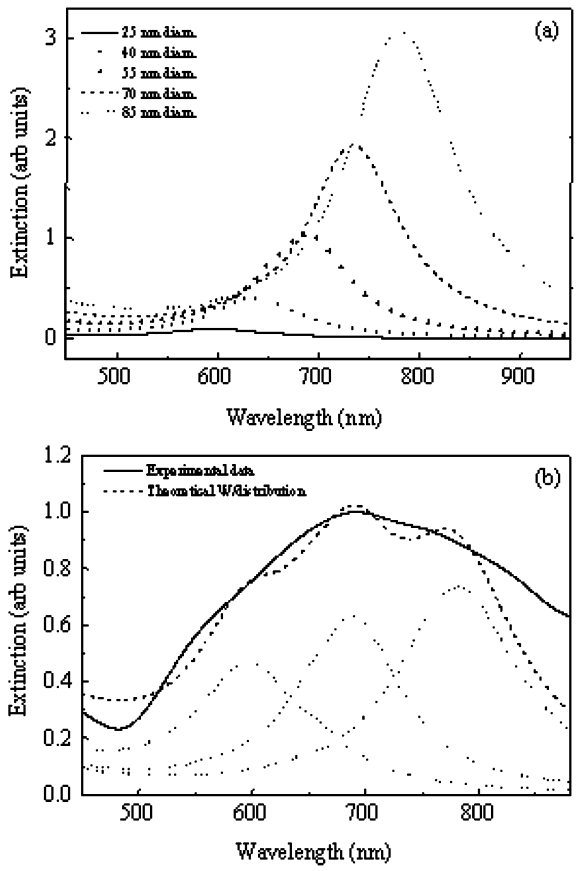

Figure 9. Normal incidence extinction spectra (a) calculated for nanocaps with $r = 50$ nm, $t = 12.5$ nm, and various diameters, d. (b) A theoretical fit to the experimental normal incidence spectrum ($\theta = 0°$) from Figure 6a using a distribution of nanocaps with $r = 50$ nm, $t = 12.5$ nm, and $d = 25$, 55, and 85 nm. The relative proportions of the three nanocap diameters in the distribution are 34.5 to 6.4 to 2.8. The dotted curves show the individual contributions of each cap size to the total spectrum.

distribution of nanocap particles above the PDMS substrate is 14.9 nm, which is consistent with SEM and AFM observations.

Conclusion

In conclusion, we have developed a general synthetic strategy for producing reduced-symmetry plasmonic nanoparticles and have applied this straightforward approach to the fabrication of nanocups and nanocaps. We have studied the optical response of these nanostructures as a function of their orientation dependence with respect to the angle of light incidence and polarization. This synthetic strategy may also apply to the fabrication of more complex reduced-symmetry nanostructures, such as metallodielectric or bimetallic ampiphilic rods and spheres, which may lead to entirely new classes of optically active nanoparticles that can be manipulated by applied static or frequency dependent electric, magnetic, or optical fields. This study of the plasmon response of these two nanostructures as a function of orientation with respect to incident light is a prime example of the types of new nanoscale structure−property relationships that can be engineered into metallodielectric nanostructures by chemical means.

Acknowledgment. The authors gratefully acknowledge support for this work from The National Science Foundation, the Army Research Office, and the Robert A. Welch Foundation.

References and Notes

(1) Homola, J.; Yee, S. S.; Gauglitz, G. *Sens. Actuators B* **1999**, 3−15.
(2) Xia, Y.; Sun, Y. *Anal. Chem.* **2002**, *74*, 5297−5305.
(3) Maier, S. A.; Brongersma, M. L.; Kik, P. G.; Atwater, H. A. *Phys. Rev. B* **2002**, *65*, 193408.
(4) Maier, S. A.; Kik, P. G.; Atwater, H. A. *Appl. Phys. Lett.* **2002**, *81*, 1714−1716.
(5) Zacher, T.; Wischerhoff, E. *Langmuir* **2002**, *18*, 1748−1749.
(6) Lu, Y.; Yin, Y.; Li, Z. Y.; Xia, Y. *Nano Lett.* **2002**, *2*, 785−788,.
(7) Aden, A. L.; Kerker, M. *J. Appl. Phys.* **1951**, *22*, 1242.
(8) Prodan, E.; Lee, A.; Nordlander, P. *Chem. Phys. Lett.* **2002**, *360*, 325−332.
(9) Oldenburg, S. J.; Westcott, S. L.; Averitt, R. D.; Halas, N. J. *J. Chem. Phys.* **1999**, *111*, 4729−4735.
(10) Jackson, J. B.; Westcott, S. L.; Hirsch, L. R.; West, J. L.; Halas, N. J. *Appl. Phys. Lett.* **2003**, *82*, 257−259.
(11) Oldenburg, S.; Averitt, R. D.; Westcott, S.; Halas, N. J. *Chem. Phys. Lett.* **1998**, *288*, 243−247.
(12) Oldenburg, S. J.; Jackson, J. B.; Westcott, S. L.; Halas, N. J. *Appl. Phys. Lett.* **1999**, *75*, 2897.
(13) Jackson, J. B.; Halas, N. J. *J. Phys. Chem. B* **2001**, *105*, 2743.
(14) Gittins, D. I.; Susha, A. S.; Schoeler, B.; Caruso, F. *Adv. Mater.* **2002**, *14*, 508−512.
(15) Kaganer, E.; Pogreb, R.; Davidov, D.; Willner, I. *Langmuir* **1999**, *15*, 3920−3923.
(16) Graf, C.; van Blaaderen, A. *Langmuir* **2002**, *18*, 524−534.
(17) Sun, Y.; Mayers, B. T.; Xia, Y. *Nano Lett.* **2002**, *2*, 481−485.
(18) Love, J. C.; Gates, B. D.; Wolfe, D. B.; Paul, K. E.; Whitesides, G. M. *Nano Lett.* **2002**, *2*, 891−894.
(19) Taflove, A.; Hagness, S. C. *Computational electrodynamics: The finite-difference time-domain method*, Bk&Cd ed.; Artech House: Norwood, MA, 2000.
(20) Stöber, W.; Fink, A. *J. Colloid Interface Sci.* **1968**, *26*, 62−69.
(21) van Blaaderen, A.; Vrij, A. *J. Colloid Interface Sci.* **1993**, *156*, 1−18.
(22) Westcott, S. L.; Oldenburg, S. J.; Lee, R. T.; Halas, N. J. *Langmuir* **1998**, *14*, 5396−5401.
(23) Duff, D. G.; Baiker, A.; Edwards, P. P. *Langmuir* **1993**, *9*, 2301−2309.
(24) El-Sayed, M. A. *Acc. Chem. Res.* **2001**, *34*, 257−264.
(25) Westcott, S. L.; Jackson, J. B.; Radloff, C.; Halas, N. J. *Phys. Rev. B* **2002**, *66*, 155431.
(26) Chang, S.-S.; Shih, C.-W.; Chen, C.-D.; Lai, W.-C.; Wang, C. R. C. *Langmuir* **1999**, *15*, 701−709.
(27) Foss, C. A.; Hornyak, G. L.; Stockert, J. A.; Martin, C. R. *J. Phys. Chem.* **1994**, *98*, 2963−2971.
(28) Link, S.; Mohammed, M. B.; El-Sayed, M. A. *J. Phys. Chem. B* **1999**, *103*, 3073−3077.
(29) Wiesner, J.; Wokaun, A. *Chem. Phys. Lett.* **1989**, *157*, 569.